JOURNAL OF MATERIALS SCIENCE 26 (1991) 2467–2476

Pull-out and fragmentation in model fibre composites

A. N. GENT, G. L. LIU
College of Polymer Science and Polymer Engineering, University of Akron, Akron, OH 44325-0301, USA

An experimental study has been carried out of debonding and fibre rupture in model composites. A single glass rod or fibre was embedded in the centre of a long transparent silicone rubber block. Strains in the rubber in close proximity to the rod or fibre were measured as the specimen was slowly stretched. Pull-out forces, strain distributions, and debonded lengths are compared with the predictions of a simple theory based on a fracture energy criterion for debonding, and taking into account friction at the debonded interface. Experiments were carried out with rods of different diameter, rubber blocks of varied cross-section, and with two levels of adhesion. By extrapolating the debonded length to zero, values of the debonding force in the absence of friction were obtained. They were in accord with fracture energies of about 50 J/m^2 for weak bonding and about 200 J/m^2 for strong bonding. Fibre fragmentation lengths were measured also. They were in reasonable agreement with the inferred fracture energies and the measured frictional properties of silicone rubber sliding on glass. In a separate study, it was found that the frictional stress between cast silicone rubber and glass was approximately constant, about 0.1 MPa, rather than proportional to pressure, for pressures exceeding about 0.02 MPa. This feature is attributed to a particularly smooth interface between the two materials.

1. Introduction

Models of composites are widely used to test the strength of adhesion between resin and fibre. Many test methods have been adopted. We deal here with two: fibre pull-out and fibre fragmentation. Theoretical treatments have been developed in both cases, based on energy or stress criteria for debonding, i.e., assuming either that failure occurs at a critical rate of release of strain energy, designated the adhesive fracture energy G_a, or that it occurs at a critical value of interfacial shear stress τ_i.

In a pull-out test, Fig. 1, a fibre is embedded partway in a block of matrix and the force required to pull it out is determined. For a relatively stiff fibre embedded in a soft matrix, the pull-out force F provides both the fracture energy G_a and strain energy in the newly debonded portion of the matrix. Griffith's energy criterion then yields the result [1, 2]

$$F^2 = 4\pi A r E_m G_a \qquad (1)$$

where E_m is Young's modulus for the matrix material, assumed to be linearly elastic, r is the fibre radius, and A is the cross-sectional area of the sample.

This relation has been compared with experimental results for steel cords embedded in rubber blocks [1]. For a wide range of values of cord radius, size of rubber block, Young's modulus of rubber, and embedded depth of cord, reasonably good agreement was found between inferred values of adhesive fracture energy and those measured directly with a peel test for a layer of the same rubber adhering to a flat steel surface.

Similarly, for a relatively soft, linearly elastic fibre embedded in a hard, inextensible matrix, the solution is [3–5]

$$F^2 = 4\pi^2 r^3 E_f G_a \qquad (2)$$

where E_p is Young's modulus of the fibre. Piggott *et al.* considered the general case when significant deformations occur in both the fibre and the matrix [6]. They related the fracture surface energy $2\pi r L G_a$ to the stored energy in the fibre and matrix and obtained the result

$$F^2 = 4\pi^2 r^2 n E_f G_a L, \qquad (3)$$

where

$$n^2 = \left(\frac{E_m}{E_f}\right)(1 - \nu_m)\ln\left(\frac{R}{r}\right).$$

The term L denotes the fibre embedded length and R is the effective radius of the surrounding matrix, ν_m is Poisson's ratio for the matrix. Because Equation 3 arises from equating total energies, rather than the rate of energy release as a debond grows, it is not considered here to be a valid result of fracture mechanics. However, it differs from other pull-out theories by introducing the embedded length L explicitly.

In the following section, the analysis leading to Equation 1 is extended to include the work of frictional sliding. This also introduces the debonded length, and hence the embedded length L, explicitly. In

0022–2461/91 $03.00 + .12

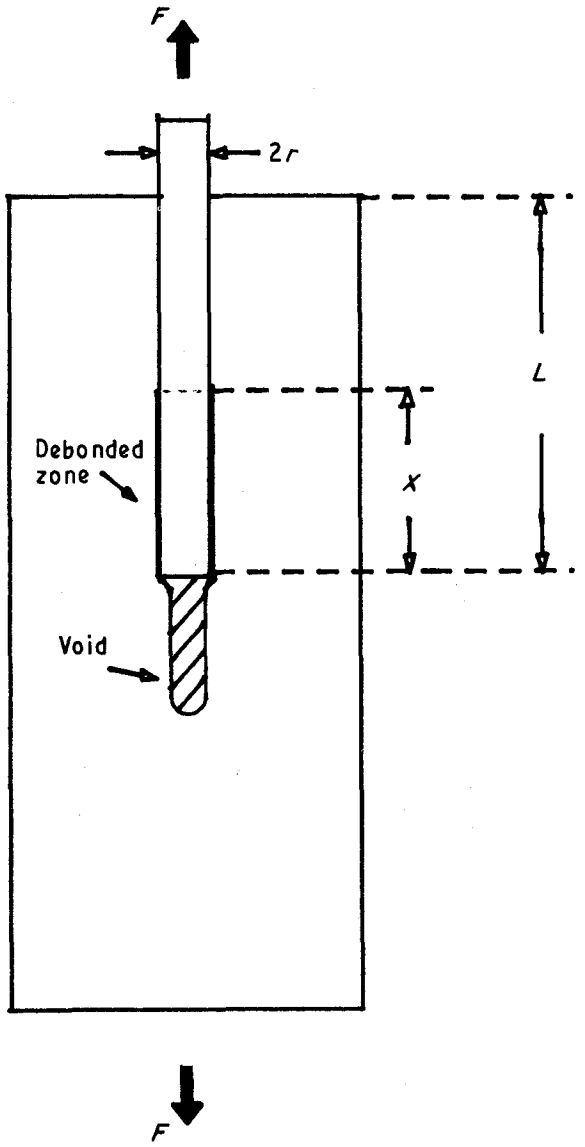

Figure 1 Pull-out of a rigid rod showing debonded zone of length X.

later sections, experimental measurements of pull-out and friction are reported for glass fibres embedded in soft rubber blocks.

The fibre fragmentation test, Fig. 2, was introduced by Kelly and Tyson [7] and has been widely employed to measure adhesion between a resin and a fibre [8–13]. A tensile force is applied to a long resin block with a single long fibre embedded along its axis. Successive fractures of the fibre take place as the specimen is stretched until the stress transferred from the matrix is no longer large enough to break the fibre again. The average final length l of fibre fragments is taken as an inverse measure of the interfacial shear strength τ_i

$$3l/4r = \sigma_b/\tau_i \quad (4)$$

where r is the fibre radius and σ_b is its tensile breaking stress. (The numerical factor 3/4 allows for a distribution of broken fragment lengths.)

Fibre fragmentation tests have been performed on a large variety of materials: glass fibre/Nylon 6, glass fibre/polypropylene and glass fibre/high density polyethylene [8]; glass fibre/epoxy [9, 10]; and carbon fibre/epoxy [11–13].

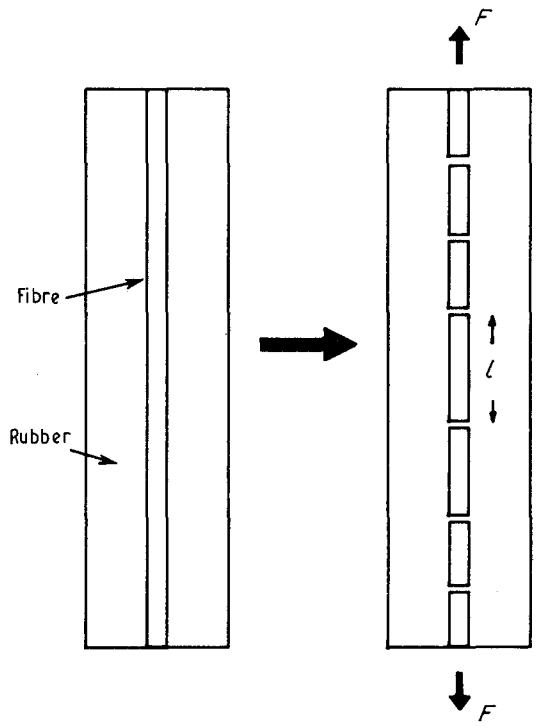

Figure 2 Fragmentation of a brittle fibre in an elastic matrix.

The fragment length l was found to be reduced when a coupling agent was applied to the fibre surface to enhance the adhesion and it was increased when specimens were tested at a higher temperature or exposed to boiling water for a period of time, in accordance with expected changes in adhesion.

However, the theoretical understanding of fragmentation is somewhat unsatisfactory because there is no independent way of measuring τ_i. Moreover, although the result, Equation 4, has been widely used, it has not been subjected to a critical experimental test. An energy criterion for failure at the resin–fibre interface, followed by fibre rupture, is employed here instead. Experimental measurements are described for a model system consisting of a single glass fibre embedded along the central axis of a long transparent silicone rubber block. They are compared with the results of pull-out experiments, where a glass fibre is embedded partway into a rubber block and pulled out by a tensile force. Different levels of adhesion between the glass fibre and the rubber have been employed, and a wide range of fibre diameter and size of rubber block, in order to test the proposed mechanism of fragmentation comprehensively.

An essential feature of the mechanics of breaking an embedded fibre into many fragments is that the force applied to a fibre fragment must rise up to the breaking force of the fibre *again*, after fibre rupture has already occurred. Thus, as debonding continues along a fragment of fibre, the force required to propagate the debond must increase continuously. This feature can be observed in experimental measurements of the force applied during fragmentation. It implies that an additional mechanism enters into the debonding process, other than the work of debonding, which would be expected to remain constant as debonding proceeds.

One possible cause of additional work is frictional sliding between detached portions of the fibre and resin. Friction can contribute significantly to the apparent work of detachment. For example, an externally applied pressure has been shown to increase the pull-out force dramatically [14, 15]. The contribution of friction is especially large for deeply embedded and large-diameter inclusions [5]. Moreover, it increases as debonding continues and the length over which sliding takes place increases [5, 16]. In experiments with steel rods or cords embedded in rubber blocks, large frictional contributions to the measured pull-out force were found [5, 16, 17]. A similar comparison is attempted here for glass fibres embedded in a silicone rubber block. In this case, independent measurements have been made of both the frictional properties of the interface and the strength of adhesion.

Measurements have been made of the distribution of stresses and strains within the rubber while a debond propagates along the fibre, starting at one end. They are compared with the predictions of a simple pull-out theory based on a fracture energy criterion for debonding, including friction. By extrapolating the debonded length to zero, values of the debonding force in the absence of friction were obtained.

Fibre fragmentation lengths were measured also. They are compared with the pull-out results and employed to derive fracture energies in the final part of the paper.

2. Theoretical considerations

A simple energy balance between work done by the applied force, energy expended in debonding, and elastic energy stored in the newly debonded material, leads to Equation 1. In order to include work expended in frictional sliding as well, we consider the increment in pull-out force, ∂F, due to friction:

$$\partial F = 2\pi r \mu p \partial X \tag{5}$$

where r is the fibre radius, μ is the coefficient of friction, p is the compressive stress and X is the debonded length. If the compressive stress is set up by frustrated Poissonian contraction of an incompressible elastic matrix material, in the form of a thin tube surrounding the fibre, then p is given by

$$p = F/3\pi a^2 \tag{6}$$

where a is the outer radius of the tube. On integration, the relation between pull-out force F and debonded length X is obtained as [16]

$$ln(F/F_0) = 2\mu r X/3a^2. \tag{7}$$

where F_0 is the pull-out force for a debonded length X of zero. This result is based on the assumption that the coefficient of friction, μ, is constant. But, as shown in the Appendix, the frictional properties of silicone rubber sliding over a smooth glass surface were found to be rather unusual. For pressures greater than about 2 per cent of Young's modulus E of the rubber, the frictional stress was found to be *independent* of pressure, rather than proportional to it.

In the pull-out and fragmentation experiments the experimentally-measured tensile strain at the debond tip was always larger than 0.04, and the corresponding compressive stress set up by frustrated Poissonian contraction in the rubber was thus always greater than $0.02E$. Under all of the experimental conditions encountered in the present experiments, therefore, the product μp can be assumed to be a constant k, independent of the magnitude of the normal stress p. On integrating Equation 5 subject to this condition, the pull-out force is obtained as

$$F = 2\pi r k X + F_0. \tag{8}$$

Thus, a linear relationship is predicted to hold between pull-out force F and debonded length X. By extrapolating the measured pull-out force F as a function of debond length to the case when $X = 0$, i.e., in the absence of a frictional contribution, the intercept F_0 yields the strength of adhesion G_a by means of Equation 1. Experimental measurements of matrix strain as a function of location, debond length, and applied force are compared with the predictions of Equations 1 and 8 in later sections of this paper, and values of G_a are deduced from them.

3. Experimental details

3.1. Materials

Elastic resins were prepared by mixing Sylgard S-184 liquid silicone resin (10 parts) and Sylgard C-184 curing agent (1 part), both provided by Dow Corning Co. The mixture was degassed at room temperature and then cured to form a transparent elastic matrix material, as indicated in Table I. Young's modulus E of the cured material was taken from the initial slope of a tensile stress–strain relation, measured at a strain rate of about 2×10^{-4}/s.

Glass rods of various diameters from 80–800 μm were prepared from Pyrex glass, and glass fibres, having a diameter of about 10 μm were obtained from Owens Corning. Glass plates, used as control surfaces, consisted of microscope slides (Fisher Scientific Company, Cat. No. 12-550A.) All the glass surfaces were cleaned with sulphuric acid, washed, dried, and then treated in one of two ways: either with a 50 per cent solution of a silane coupling agent (Primer 92-023, Dow Corning Co.) in hexane, to promote bonding to the silicone resin; or with a 1 per cent solution of phenyl isocyanate in anhydrous ether, to react with hydroxyl groups on the glass surface and thus minimize bonding to the silicone resin.

3.2. Pull-out experiments

Surface-treated glass rods were first coated with a thin layer of silicone resin, which was partially cured for 1

TABLE I Young's moduli E of matrix materials

Resin	Cure temperature (°C)	Time (h)	E (MPa)
A	110	12	2.8
B	80	12	2.5
C	23	168	1.2

hour at 23 °C. A series of red dots was then applied along the length of the fibre, at 3 mm intervals, using a paste made up of red dye, Cabosil powder (Cabot Corporation), and silicone resin, in order later to carry out measurements of strains set up in the resin in close proximity to the fibre.

In some cases it was desired to vent to air the cavity formed at the end of a rod during pull-out experiments. A length of fine copper wire was then adhered to the end of the glass rod before it was covered with resin.

Specimens were prepared with two cross-sections: circular, using a plastic straw as a mould, 100 mm long and 5.25 or 6.25 mm in diameter; and rectangular, by cutting parallel-sided strips from a sheet made in a mould, 100 mm in width, 150 mm in length, and 2–8 mm in height. In the first case, a glass rod was placed in the centre of the cylindrical cavity and uncured silicone resin was poured around it. In the second case, the mould was half filled with resin which was then slightly cured at 23 °C for 4 hours. Then, several fibres or marked glass rods were placed parallel to each other on the surface of the resin and the remainder of the resin was added, covering the fibres or rods and filling the mould. Strips were cut so that a single glass rod or fibre was centrally located along the axis. The cross-sectional area of the strips varied from about 1.5 × 2 mm to about 4 × 8 mm.

Curing was completed at the temperatures and for the times listed in Table I. After curing, the fine copper wire, if used, was pulled out, leaving an air channel leading from the exterior to the end of the rod or fibre.

No significant differences were found in the pull-out behaviour for samples with different shapes of cross-section. On the other hand, the size of the cross-sectional area had a strong effect on the pull-out force, as described later.

The initial distance between red dots in the resin near the glass fibre was measured with a low-power microscope. Then, as the sample was stretched, the applied tensile force and the distance between dots were measured simultaneously, at convenient intervals. Stretching was imposed at about 10 μm/s on samples having initial lengths between 60 and 100 mm.

The critical strain at which debonding began at the fibre or rod tip was determined by measuring the distance between two marks on the surface of the sample just below the end of the glass rod as a debond was seen to initiate at the tip and propagate along the rod.

3.3. Fragmentation experiments

Fine glass fibres, about 10 μm in diameter, or glass rods, were placed in a horizontal mould which was then filled with degassed silicone resin and cured using the conditions listed in Table I. Samples were stretched at rates of 10 μm/s or 1 mm/s and stretching continued until it was clear that the fibre had been fully fragmented. The lengths of fibre fragments were then measured with a microscope at magnifications of 30 × or 100 ×, while the sample was held stretched.

3.4. Determination of adhesive and cohesive fracture energies

Silicone resin was cast as a sheet, about 1.5 mm thick, on the treated surface of a glass microscope slide and cured at temperatures of 23 °C or 80 °C. A strip of muslin cloth was adhered to the surface to prevent the silicone layer from stretching during detachment. The adhesive fracture energy G_a was calculated from measurements of peel force F for peeling the silicone resin strip away at a peel angle θ of 45°, Fig. 3:

$$G_a = F(1 - \cos\theta)/w \quad (9)$$

where w is the width of the strip.

Similarly, the cohesive fracture energy G_c was calculated from the tearing force F and the width t of the tear for a sheet of resin, about 1.5 mm thick, torn apart by pulling half-sections away from each other at 180°, Fig. 4, at a speed of 10 μm/s.

$$G_c = 2F/t. \quad (10)$$

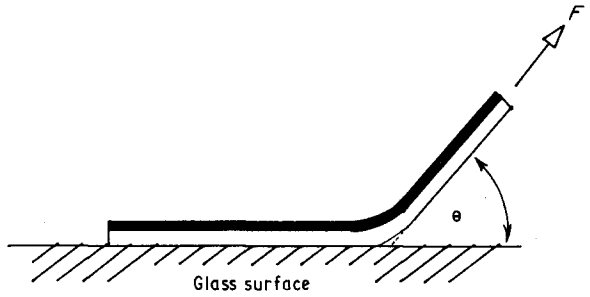

Figure 3 Measurement of adhesive fracture energy by peeling.

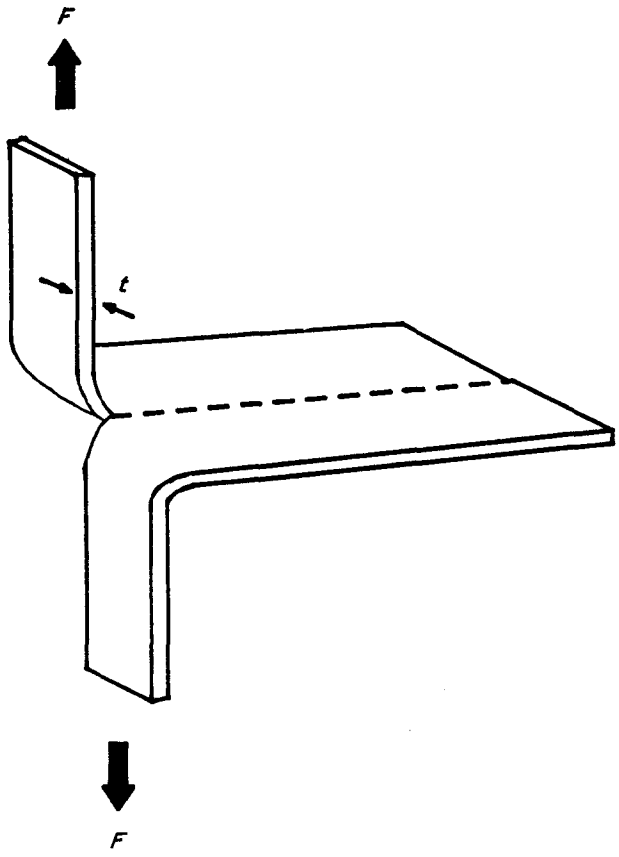

Figure 4 Measurement of cohesive fracture energy by tearing.

The torn width t was measured with a microscope after the test. The tear generally ran at an angle of about 45° to the thickness of the sheet.

3.5. Determination of frictional coefficient for silicone resin sliding against glass

For frictional measurements at low contact pressures, a block of silicone rubber, 20 mm in length, 10 mm in width, and 1 mm in thickness, was adhered to the lower surface of an aluminium sled, pressed against a horizontal flat glass surface and towed over it at a speed of about 10 μm/s. For higher contact pressures, several short rods with domed-top surfaces, having a radius of about 3 mm, were adhered to the aluminium sled, pressed simultaneously against the glass surface, and pulled over it. In this case, the total contact area for the set of circular contact regions was measured through the glass, with a microscope.

The frictional force F was measured for various values of normal force N, and the frictional coefficient μ was calculated from the ratio

$$\mu = F/N. \tag{11}$$

Results are given in the Appendix.

4. Results and discussion

4.1. Fibre pull-out: experimental observations

A typical force–displacement curve for fibre pull-out is shown in Fig. 5. At a sufficient force, i.e., when the strain at the debond tip reached a critical value and the strain energy was high enough, a debond was seen to propagate for a distance of about 0.3 mm along the interface. Simultaneously, a drop in force could be observed in the force–displacement curve. The pull-out force then increased with increasing displacement and increasing length of debond. This stick–slip process repeated itself as the sample was continuously stretched and the debond propagated along the fibre.

Growth of the debond could be observed with a microscope by the appearance of some small spots at the interface when the rubber became detached from the surface of the glass rod. For a small rod embedded in, and strongly bonded to, a large block of rubber, the rate of propagation of the debond was relatively high (greater than about 30 μm/s) and the debonding could be observed very clearly under the microscope. But for a sample with a low rate of debonding or with weak adhesion, the stick–slip process was much slower and the spots were not evident. In this case, the location of the debond tip was determined from the experimentally measured strain distribution, as described below.

The strain measured at the debond tip fluctuated along with the stick–slip failure process. The highest value of strain observed was taken as the critical level of strain in the matrix at the site of debonding. It was about 0.12 for a typical strongly bonded specimen.

4.2. Fibre pull-out: strain distribution in the matrix

Distances between red dots near the fibre surface were measured during pull-out and the corresponding tensile strains calculated. Typical strain distributions are shown in Fig. 6. The location of the end of the glass fibre is denoted at $x = 0$. The $-x$ direction indicates distance along the rubber block past the end of the fibre. The strain here was uniform, of course. The $+x$ direction denotes distance along the fibre. Here, the strain in the debonded region appeared to vary linearly with distance from the fibre end up to the debond tip, indicated by the vertical broken line in Fig. 6. Past this point, the strain in the rubber was effectively zero.

As the applied load was increased, the debonded length increased and the strain distribution shifted linearly to higher levels (Fig. 6). The measured strain distributions are replotted in Fig. 7 against the distance x' from the tip of the debond, for different levels of pull-out force. All of the data are seen to fall on a single line in this representation, in accordance with Equation 8, when the frictional stress μp is constant. As the debonded length increased, a proportionally higher force was needed to overcome the increasingly large frictional contribution.

The intercept of a plot of strain versus the length X of the debond corresponds to the pull-out force F_0 associated with the bond strength at the interface in the absence of friction (Equation 1).

A systematic study of pull-out forces was carried out using well-bonded glass rods of various diameters. In all cases, a plot of pull-out force versus debonded

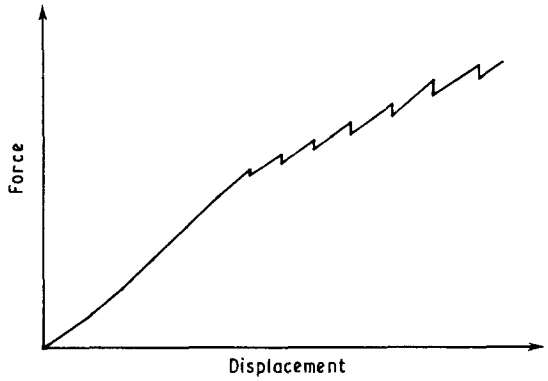

Figure 5 Sketch of force–displacement relation for fibre pull-out.

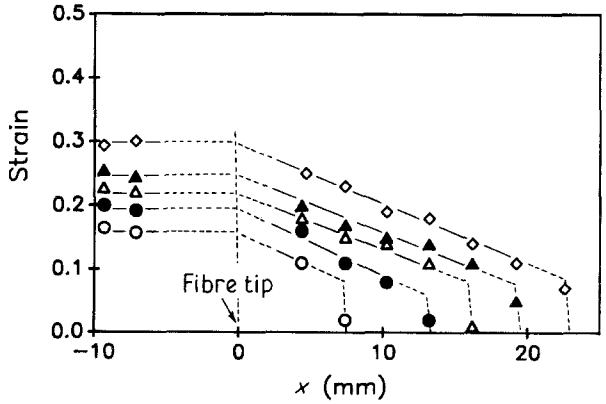

Figure 6 Variation of tensile strain in the elastic matrix with distance x from the tip of a well-bonded embedded fibre. F = 900 g, ◇; 753 g, ▲; 683 g, △; 570 g, ●; 472 g, ○.

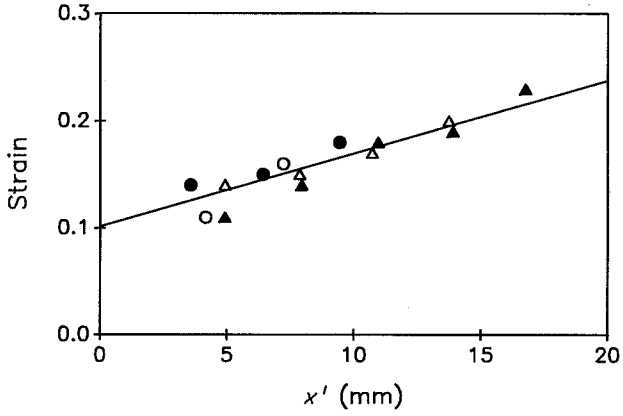

Figure 7 Tensile strains in the elastic matrix plotted as a function of the distance x' from the debond front. Results taken from Fig. 6. F = 900 g, ▲; 753 g, △; 683 g, ●; 570 g, ○.

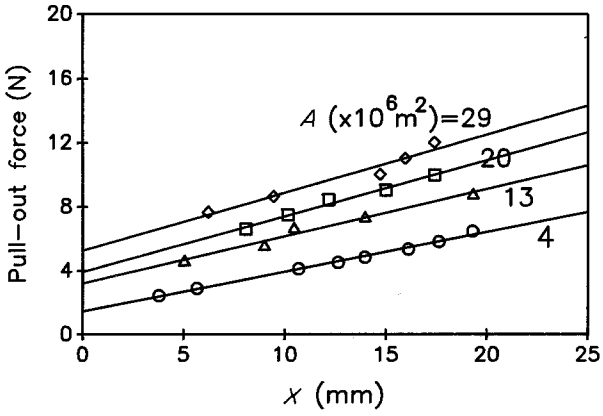

Figure 9 Pull-out force versus length of debond for a well-bonded rod (180 μm diameter) embedded in resin blocks of various cross-sectional areas A.

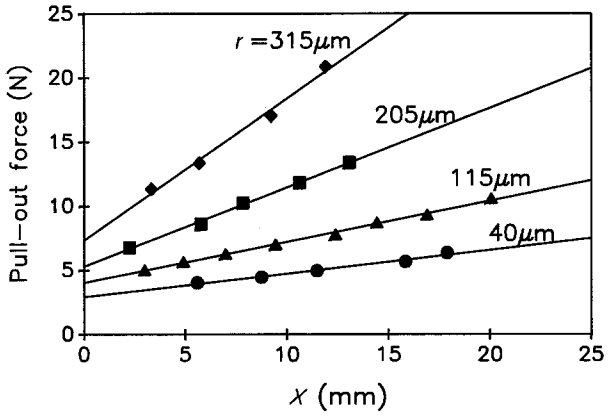

Figure 8 Pull-out force versus length of debonded zone for well-bonded rods of various radii r.

length gave a straight line in agreement with Equation 8. Results are shown in Fig. 8 for rod diameters of 80 μm to 630 μm, embedded in rubber blocks with a cross-sectional area of about 22 mm^2. The slope of the plot of pull-out force versus debonded length increased substantially, from 0.18 to 1.11 N/mm, as predicted by Equation 8. The intercept force F_0 increased with both fibre diameter and sample area.

On the other hand, when the cross-sectional area of the rubber block was changed from 4 to 29 mm^2, about 7 times larger, the slope of the plot of pull-out force versus debonded length for a fibre of diameter 180 μm was more or less constant, as shown in Fig. 9. These effects of fibre diameter and area of block cross-section on pull-out force are in good agreement with the predictions of Equation 8.

Values of k (= μp) and adhesive fracture energy G_a were calculated from the slope and intercept of plots of pull-out force versus debonded length, using Equation 8. They are given in Table II. A consistent value for μp was obtained of 0.53 ± 0.08 MPa, but this is much larger than the value measured directly in frictional sliding experiments which was only about 0.1 MPa (see Appendix). The discrepancy may be due to differences in surface roughness [18, 19].

Values of adhesive fracture energy G_a were calculated from F_0, using Equation 1. The value obtained was 210 ± 30 J/m^2. A directly measured value could not be obtained for these strongly bonded specimens using peel tests. The rubber sample broke instead of detaching because the adhesive strength was large, close to the cohesive strength of the rubber, which was found to lie in the range 245–350 J/m^2. Thus, a pull-out test provides a possible method to measure adhesive strength when other methods lead to cohesive rupture.

TABLE II Pull-out results for well-bonded rods

Resin area A (mm^2)	Rod diameter d (μm)	Slope πdk (N/mm)	Intercept F_0 (N)	Calculated $\mu p = k$ (MPa)	Calculated G_a (J/m^2)
4.05	180	0.25 ± 0.07	1.4 ± 0.1	0.44	160
10.68	215	0.36 ± 0.02	2.9 ± 0.2	0.53	210
13.16	185	0.30 ± 0.03	3.2 ± 0.3	0.52	240
22.19	80	0.18 ± 0.01	2.9 ± 0.2	0.72	270
19.58	180	0.35 ± 0.02	3.9 ± 0.3	0.62	250
21.07	230	0.32 ± 0.08	4.0 ± 0.1	0.44	190
22.42	360	0.55 ± 0.02	5.4 ± 0.2	0.49	200
19.52	410	0.62 ± 0.02	5.3 ± 0.2	0.48	200
23.79	630	1.11 ± 0.07	7.3 ± 0.6	0.56	200
31.74	315	0.53 ± 0.03	5.5 ± 0.4	0.54	170
			Average	0.53 ± 0.08	210 ± 30

4.3. Effect of external pressure

Under extension, a large void formed at the end of the fibre. The question arises: how much effect does the pressure differential between the external atmosphere and the vacuum within the void have on the pull-out force? By allowing air to enter the void through a fine hole, the vacuum within it could be relieved. Samples were studied with and without such an air path. The results are shown in Fig. 10, where closed symbols denote unvented samples and open symbols denote samples with an air channel. In all cases, a straight line relationship was obtained between pull-out force and debonded length. Venting the debond cavity to the atmosphere only caused a slight decrease in pull-out force for both fibre diameters employed; 440 and 290 μm, and weakly bonded samples behaved in the same way as well-bonded ones (Table III). Thus, the effect of the vacuum set up at the end of the fibre appears to be slight. This is probably because, for these materials, frictional stresses are largely independent of applied pressure. A greater effect of atmospheric pressure would be expected for materials that show Coulombic frictional behaviour.

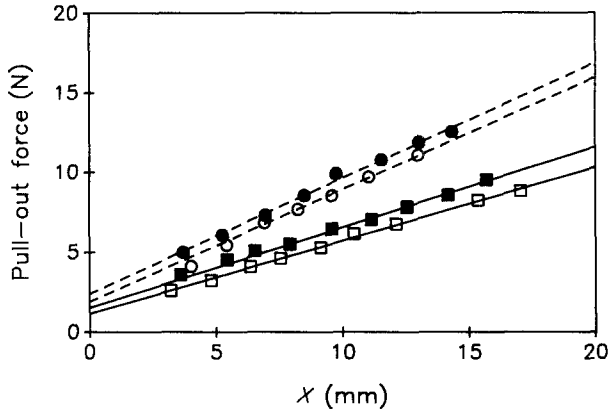

Figure 10 Pull-out force versus length of debond for weakly bonded rods embedded in elastic blocks. Circles: rod diameter $d = 440$ μm; squares: $d = 290$ μm. Open symbols are for specimens with an air channel from the rod tip to the external atmosphere.

4.4. Comparison of values of friction stress and fracture energy G_a for different systems

Values of k ($= \mu p$) and G_a were calculated from the slope and intercept of experimental relations between pull-out force and debonded length for weakly bonded samples. The values are listed in Table III. For samples cured at room temperature the average value of μp was 0.52 ± 0.02 MPa, similar to that obtained before for strongly bonded samples. Thus, the frictional stress μp was found to be consistent in all cases. For the weakly bonded samples the average value of the adhesive fracture energy G_a was 48 J/m^2, considerably smaller than for the samples prepared with an adhesion promoter. Even smaller values, about 40 J/m^2, were obtained with a somewhat stiffer rubber resin, having a value of Young's modulus of 2.5 MPa (Table III).

Values of the adhesive fracture energy for weakly bonded samples were determined by peeling measurements. (Strongly bonded samples broke instead of detaching.) The results are given in Table IV and compared with values deduced from pull-out experi-

TABLE IV A comparison of values of G_a (J/m^2)

(1) Strong bonding (silane-treated glass)

Pull-out	Fragmentation
210 ± 30	210 ± 30

(2) Weak bonding (phenyl-isocyanate treated glass)

	Pull-out	Fragmentation	Peel
Resin A	48 ± 5	50 ± 25	51 ± 8
Resin B	40 ± 8	—	44 ± 6

TABLE III Effect of external pressure on pull-out

Area A (mm^2)	Diameter d (μm)	Slope πdk (N/mm)	Intercept F_0 (N)		Calculated $\mu p = k$ (MPa)	Calculated G_a (J/m^2)
Resin A ($E = 1.2$ MPa)						
21.6	290	0.50 ± 0.09	1.5 ± 0.1		0.55 ± 0.02	50 ± 8
[a]21.6	290	0.46 ± 0.01	1.2 ± 0.1		0.50 ± 0.02	28 ± 5
25.5	440	0.72 ± 0.02	2.4 ± 0.2		0.52 ± 0.02	69 ± 15
[a]25.5	440	0.70 ± 0.03	1.9 ± 0.2		0.51 ± 0.02	44 ± 10
				Average	0.52 ± 0.02	48 ± 15
Resin B ($E = 2.5$ MPa)						
25.5	510	0.82 ± 0.01	3.3 ± 0.2		0.51 ± 0.02	53 ± 8
[a]25.5	510	0.76 ± 0.02	3.1 ± 0.2		0.47 ± 0.02	45 ± 8
35.0	570	0.99 ± 0.02	3.6 ± 0.3		0.55 ± 0.02	41 ± 7
36.0	600	1.09 ± 0.03	3.6 ± 0.3		0.58 ± 0.02	38 ± 7
36.0	760	1.15 ± 0.06	3.5 ± 0.6		0.48 ± 0.03	28 ± 10
47.5	570	1.10 ± 0.06	4.0 ± 0.6		0.61 ± 0.03	37 ± 11
				Average	0.53 ± 0.05	40 ± 8

[a]Sample with a hole to air.

TABLE V Pull-out results for fine silane-treated fibres

Resin area A (mm^2)	Fibre diameter d (μm)	Debond force F_0 (g)	Calculated G_a (J/m^2)
1.64	8.8	29.7	305
1.78	10.1	28.0	180
2.05	9.2	34.2	337
2.65	10.7	33.5	222
3.64	9.5	46.0	334
3.74	10.9	41.0	225
		Average	270 ± 60

ments. For resin A, a soft rubber, the adhesive fracture energy from pull-out was 48 J/m^2, and that from peeling was 51 J/m^2. For resin B, a stiffer rubber, the adhesive fracture energy from pull-out was 40 J/m^2 and that from peeling was 44 J/m^2. Thus, fairly good agreement was obtained.

There are special difficulties in carrying pull-out experiments with fine glass fibres, with a diameter of only 10 μm. Details of the failure process are hard to see on such a small scale. In particular, it proved difficult to determine the debonded length. In this case, therefore, the initial pull-out force F_0 was taken as the maximum force reached before a small drop occurred in the experimental force–displacement relation. The adhesive fracture energy G_a was estimated from this initial force F_0 and the results are given in Table V. The average value obtained for G_a was 270 ± 60 J/m^2, slightly larger than for previous samples using larger-diameter glass rods. This may be due to the higher rate of debond propagation observed with a fine fibre embedded in a large block of rubber, causing a higher adhesive fracture energy.

4.5. Fragmentation tests: experimental observations

When a sufficiently large tensile force is applied to a single fibre embedded in a block of rubber, it breaks and the ends of the broken fibre move apart, leaving a cylindrical void between them. Simultaneously, the applied force drops, Fig. 11. Subsequently, as the applied force is increased further, two debonds propagate along the fibre in both directions, away from the point of fracture. Eventually, the force becomes high enough to cause fracture of the fibre again, elsewhere. This process continues until the fibre is completely fragmented.

This successive stressing and debonding of the fibre before it breaks again can be considered as a series of repeated pull-out processes. In principle, therefore, pull-out theory can be applied to fibre fragmentation. Measurements were made of strain distributions in a single-fibre fragmentation sample, for comparison with those observed before.

Local strains could only be measured accurately for large-diameter fibres. An example is given in Fig. 12 for a fibre of diameter 150 μm after two fractures had occurred. The first fracture took place at the position

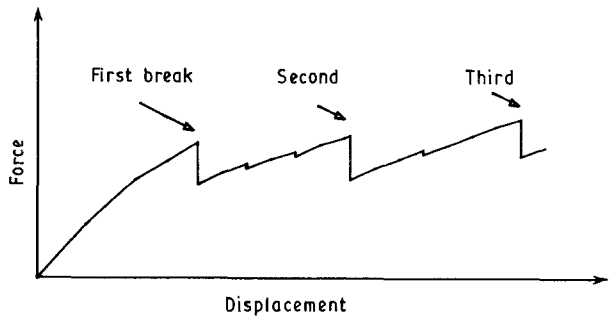

Figure 11 Sketch of the force–displacement relation in a fragmentation experiment.

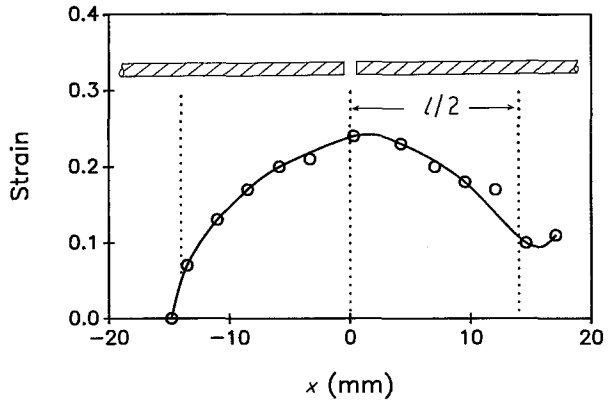

Figure 12 Tensile strain in the elastic matrix on either side of the point of second fracture of a weakly bonded rod, diameter d = 150 μm. The first fracture occurred at x = 27.6 mm.

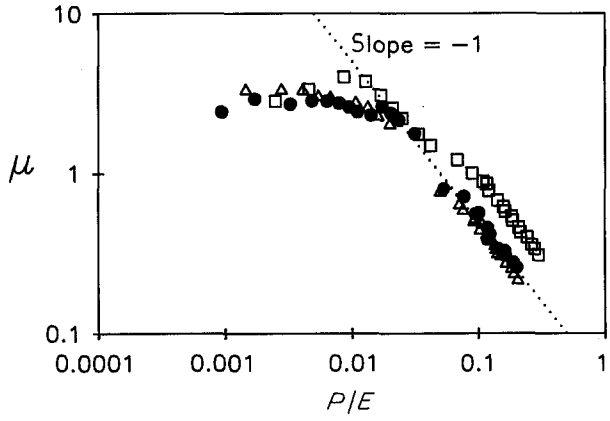

Figure 13 Dependence of the coefficient of friction μ on pressure P for silicone rubber sliding on glass. Resin A (E = 2.8 MPa), ●; B (E = 2.5 MPa), △; C (E = 1.2 MPa), □.

denoted $x = 0$, when the applied force F reached 536 g. The debond then propagated in both directions away from the fracture point until the applied force reached 543 g, when the second fracture occurred, at a point 27.6 mm away. A half-length of this fragment, 13.8 mm, is shown as $l/2$ in Fig. 13. The position marked $x \approx -14$ mm represents the debond tip because the measured strain was effectively zero after this point. Thus, the debonded length, determined from the distance between the broken end of the fibre and the tip of the debond, is almost exactly one-half of the length of the fibre fragment. It may be concluded that

TABLE VI Fragmentation tests with larger-diameter fibres: F_b is the fibre breaking force; F_d is the force right after the fibre broke

		First break		Second break				
A (mm^2)	d (μm)	F_b (g)	F_d (g)	F_b (g)	F_d (g)	l_c (mm)	F_0 (N)	G_a (J/m^2)
20.99	150	536	234	543	375	27.6	1.9 ± 0.4	113 ± 50
21.52	180	476	200	545	385	28.3	1.2 ± 0.3	50 ± 25
[a]21.09	200	—	—	662	420	31.7	1.2 ± 0.3	46 ± 23

[a]: the first fracture occurred before the test.

TABLE VII Fragmentation of silane-treated fine glass fibres

A (mm^2)	d (μm)	No. of fragments	F_b (N)	l_c (mm)	F_0 (N)	G_a (J/m^2)
2.83	10.4	3	0.57 ± 0.03	26.3 ± 10.3	0.34	223
2.72	10.9	4	0.49 ± 0.07	22.5 ± 6.6	0.28	150
2.86	10.0	6	0.52 ± 0.04	21.4 ± 6.5	0.34	230
3.10	9.3	4	0.51 ± 0.05	22.3 ± 3.8	0.33	215
2.88	10.7	6	0.54 ± 0.02	19.1 ± 5.5	0.37	2.53
2.78	10.7	5	0.48 ± 0.10	18.5 ± 6.0	0.31	184
					Average	210 ± 30

the debonded length is equal to one half of the length of a characteristic fragment when the applied force is equal to the fibre breaking force. Thus, pull-out theory explains the basic features of fragmentation.

Equation 8 relates the applied force F to the initial pull-out force F_0 and the debonded length X. Thus, the initial pull-out force F_0 can be calculated from the measured breaking force and the fragmentation length. In this calculation the constant μp was taken to be 0.5 MPa, as in the pull-out study.

The results for a soft rubber ($E = 1.2$ MPa) with a weakly bonded fibre are given in Table VI. The adhesive fracture energy calculated from F_0 was about 50 J/m^2, quite similar in magnitude to those estimated from fibre pull-out experiments.

The results of fibre fragmentation experiments for strongly bonded fibres are given in Table VII. F_0 was calculated from the fibre breaking force and fibre fragment length, using Equation 8. The adhesive fracture energy was 210 ± 30 J/m^2, in good agreement with the results from fibre pull-out experiments. These results indicate that both fibre pull-out and fragmentation have the same fracture mechanism.

To the best of the authors' knowledge, effects of sample size and test speed on fibre fragmentation have not been examined previously. They are considered together here, because it was observed that samples having larger cross-sectional areas tended to fail quickly, at higher rates of debonding. Experiments were carried out using well-bonded samples of different cross-sectional area from 3 to 5 mm^2. As the area increased, the calculated adhesive fracture energy increased significantly, from 210 to 300 J/m^2. On the other hand, when the sample area was held constant at 3 mm^2, but the test speed was increased from 0.5 to 50 mm/min, the adhesive fracture energy increased in a similar way, from 210 to 310 J/m^2. It is concluded that pull-out theory accounts satisfactorily for fibre fragmentation, including changes in sample cross-sectional area, but care must be taken to ensure that the rate of debonding is constant. Otherwise, for viscoelastic matrix materials, the fracture energy increases significantly as the rate of debonding is increased.

4.6. Values of fracture energy G_a from different experiments

A comparison of adhesive fracture energy values is made in Table IV. For strong bonding, the value was about 210 J/m^2 from both pull-out and fragmentation tests. Values for weak bonding were about 50 J/m^2 from pull-out, fragmentation and peel tests. Thus, good agreement was found between values of G_a from pull-out and fragmentation measurements, and from peeling experiments when comparison was possible.

5. Conclusions

1. A critical pull-out force F_0 was found to be necessary to initiate debonding at the end of a fibre embedded in a silicone rubber block.

2. The pull-out force then increased linearly as the length of the debond increased, indicating that a frictional effect is important.

3. The strain in the rubbery matrix increased linearly with distance from the point of initial debonding, being greatest at the fibre end.

4. The slope of plots of pull-out force versus length of debond was strongly dependent on the fibre diameter, rising from 0.18 N/mm to 1.11 N/mm as the fibre diameter increased from 80 μm to 630 μm. As the cross-sectional area of the matrix block was increased from 4 mm^2 to 29 mm^2, the intercept F_0 increased, but the slope remained more or less the same. These effects are consistent with a simple theory of pull-out, including frictional sliding.

5. In a fragmentation test, the applied force drops when the fibre breaks. Then, as the applied force is increased, debonds propagate along the fibre in both directions away from the site of fracture, until the load is sufficient to break the fibre again. Fibre fragmentation can be considered as a repeated fibre pull-out test, until all of the fragments are fully debonded.

6. The average length of fibre fragments and the average fibre breaking force allow the adhesive fracture energy G_a to be estimated from pull-out theory, when allowance is made for friction.

7. Good numerical agreement is found between values of G_a from pull-out and fragmentation measurements, and from peeling.

8. Inferred frictional stresses at the debonded interface were much larger than directly measured values. This may be due to differences in surface roughness.

Appendix: Friction between silicone rubber and glass

A study of friction was made by sliding samples of silicone rubber over a glass surface. Two kinds of rubber sample were used: a block of rubber and an assembly of rods with spherical asperities. The latter sample enabled higher normal pressures to be applied by reducing the contact area. The frictional coefficient was measured for normal pressures ranging from $0.002E$ to $0.3E$, where E is the Young's modulus of the rubber, ranging from 1–3 MPa.

The frictional coefficient was found to be strongly pressure-dependent, Fig. 13. At low contact pressures, it was more or less constant. However, when the pressure was greater than about 1–2% of the value of Young's modulus of the rubber, the values of μ decreased sharply. The results then fell on a line with a slope of -1 on a plot of $\log \mu$ versus $\log(p/E)$, i.e., the frictional shear stress, given by μp, was constant. The value of μp measured using a rubber block with a flat surface was about 0.07 MPa, and for a rubber specimen with curved surfaces it was about 0.12 MPa. This slight difference in μp may be due to edge effects with the different samples.

Acknowledgements

This work forms part of a programme of research on adhesion supported by the Office of Naval Research (Contract N00014-85-K-0222; Program Officer Dr R. S. Miller). Grants-in-aid from Westvaco, 3M, and Lord Corporation are also gratefully acknowledged. Helpful discussions with Dr W. S. Haworth of 3M Company Biomaterials Laboratory on the strength of fibre-reinforced solids inspired much of the work.

References

1. A. N. GENT, G. S. FIELDING-RUSSELL, D. I. LIVINGSTON and D. W. NICHOLSON, *J. Mater. Sci.* **16** (1981) 949.
2. R. F. BREIDENBACH and G. J. LAKE, *Phil. Trans. R. Soc.* **A299** (1981) 189.
3. C. GURNEY and J. HUNT, *Proc. R. Soc.* **A299** (1967) 508.
4. J. O. OUTWATER and M. C. MURPHY, Annual Technical Conference, 1969, Reinforced Plastics and Composities Institute **11-C** (Society of Plastics Industry) p. 1.
5. A. N. GENT and O. H. YEOH, *J. Mater. Sci.* **17** (1982) 1713.
6. M. R. PIGGOTT, A. SANADI, P. S. CHUA and D. ANDISON, in "Composite Interfaces", Proceedings of the First International Conference 1986, edited by H. Ishida and J. L. Koenig (Elsevier, New York, 1986) p. 109.
7. A. KELLY and W. R. TYSON, *J. Mech. Phys. Solids* **13(6)** (1965) 329.
8. W. A. FRASER, F. H. ACHKER and A. T. DIBENEDETTO, 30th Annual Technical Conference, 1975, Reinforced Plastics and Composites Institute **22-A** (Society of Plastics Industry) p. 1.
9. T. OHSAWA, A. NAKAYAMA, M. MIWA and A. HASEGAWA, *J. Appl. Polym. Sci.* **22** (1978) 3203.
10. A. T. DIBENEDETTO and P. J. LEX, *Polym. Engng Sci.* **29(8)** (1989) 543.
11. L. T. DRZAL, M. J. RICH, J. D. CAMPING and W. J. PARK, 35th Annual Technical Conference, 1980, Reinforced Plastics and Composites Institute **20-C** (Society of Plastics Industry) p. 1.
12. W. D. BASCOM and R. M. JENSEN, *J. Adhesion* **19** (1986) 219.
13. D. JACQUES and J. P. FAVRE, Proceedings of the International Conference on Composite Materials, Vol. 5 (1987) p. 471.
14. P. B. BOWDEN, *J. Mater. Sci.* **5** (1970) 517.
15. N. HADJIS and M. R. PIGGOTT, *J. Mater. Sci.* **12** (1977) 358.
16. A. N. GENT and S. Y. KAANG, *Rubber Chem. Technol.* **62** (1989) 757.
17. M. D. ELLUL and R. J. EMERSON, *Rubber Chem. Technol.* **61** (1988) 309.
18. M. BARQUINS and A. D. ROBERTS, *J. Phys. D: Appl. Phys.* **19** (1986) 547.
19. A. D. ROBERTS and C. A. BRACKLEY, *J. Nat. Rubber Res.* **4** (1989) 1.

Received 12 March
and accepted 20 March 1990